IEEE Photonics Journal
An IEEE Photonics Society Publication

Open Access

Ultrasensitive Temperature Sensor Based on a Fiber Fabry–Pérot Interferometer Created in a Mercury-Filled Silica Tube

Volume 7, Number 6, December 2015

Kaiming Yang
Jun He
Ying Wang
Shen Liu
Changrui Liao
Zhengyong Li
Guolu Yin
Bing Sun
Yiping Wang, Senior Member, IEEE

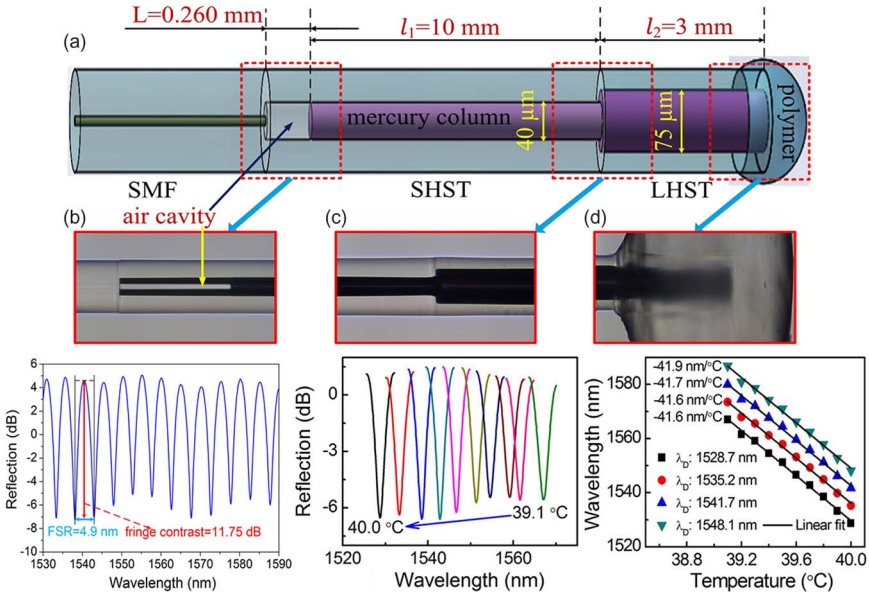

DOI: 10.1109/JPHOT.2015.2495223

Ultrasensitive Temperature Sensor Based on a Fiber Fabry–Pérot Interferometer Created in a Mercury-Filled Silica Tube

Kaiming Yang, Jun He, Ying Wang, Shen Liu, Changrui Liao, Zhengyong Li, Guolu Yin, Bing Sun, and Yiping Wang, *Senior Member, IEEE*

Key Laboratory of Optoelectronic Devices and Systems of Ministry of Education and Guangdong Province, College of Optoelectronic Engineering, Shenzhen University, Shenzhen 518060, China

DOI: 10.1109/JPHOT.2015.2495223

Manuscript received August 26, 2015; revised October 16, 2015; accepted October 20, 2015. Date of publication October 27, 2015; date of current version November 5, 2015. This work was supported by the National Natural Science Foundation of China under Grant 61505120, Grant 61425007, Grant 11174064, Grant 61377090, and Grant 61308027; by the Natural Science Foundation of Guangdong under Grant 2015A030310243, Grant 2014A030308007, and Grant 2014A030312008; by the Science and Technology Innovation Commission of Shenzhen/Nanshan under Grant GJHZ20150313093755757, Grant JCYJ20150324141711611, Grant KQCX20140512172532195, Grant ZDSYS20140430164957664, and Grant KC2014ZDZJ0008A; by the Special Fund of the Central Finance for the Development of Local Universities under Grant 000022070155; and by the Pearl River Scholar Fellowships. Corresponding author: Y. Wang (e-mail: ypwang@szu.edu.cn).

Abstract: We demonstrate an ultrasensitive temperature sensor based on a unique fiber Fabry–Pérot interferometer (FPI) that was created by means of splicing a mercury-filled silica tube with a single-mode fiber. The air cavity of the fiber FPI was formed by the surface of the mercury column and the endface of the single-mode fiber. Moreover, the mercury-based fiber FPI exhibits an ultrahigh temperature-sensitivity of up to −41.9 nm/°C, which is about one order of magnitude higher than that of the ordinary FPI-based fiber-tip sensors reported so far. Hence, such a mercury-based fiber FPI temperature sensor could be used for highly sensitive ambient temperature sensing applications.

Index Terms: Fiber optics, temperature sensor, Fabry–Pérot interferometer (FPI).

1. Introduction

Fiber-optic temperature sensors have been extensively studied due to the advantages of compact size, fast response, durability in harsh environments, and capability of remote sensing. In the past decade, numerous sensing schemes and structures have been developed for fiber-optic temperature sensors, such as fiber Bragg gratings (FBGs) [1]–[3]; long-period fiber gratings (LPFGs) [4]–[6]; liquid-filled photonic crystal fibers (PCFs) [7], [8]; in-fiber modal interferometers [9]–[12]; and fiber Fabry–Pérot interferometers (FPIs) [13], [14]. The temperature sensitivities of traditional FBGs, LPFGs, and modal interferometers are limited by the thermal-optic coefficient of fused silica and are typically less than 0.1 nm/°C. Recently, liquid-filled PCFs were explored for high sensitivity temperature sensors due to the large thermo-optic coefficient of liquid [7], [8]. For example, a fully-filled PCF and a selectively-filled PCF exhibited high temperature-sensitivities of −2.194 nm/°C and 54.3 nm/°C, respectively [7], [8]. Furthermore, temperature sensors based on fiber Mach–Zehnder modal interferometers (MZIs) were also demonstrated.

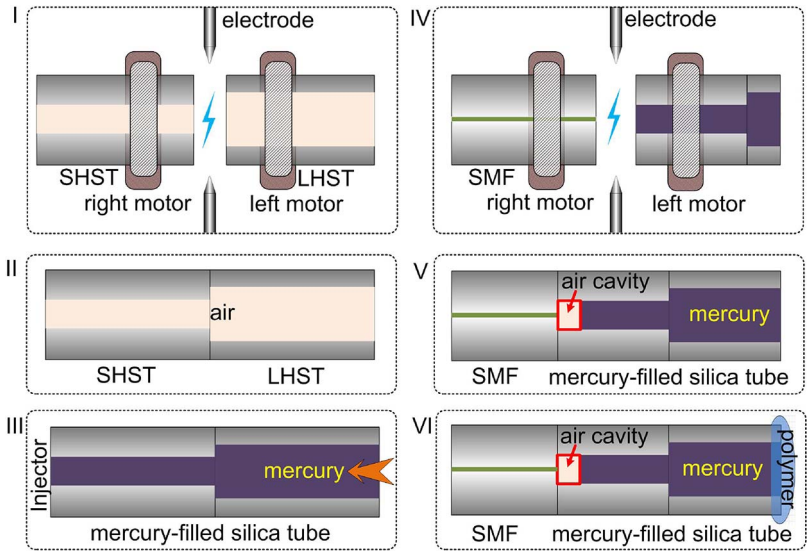

Fig. 1. Schematic diagrams of fabrication process of fiber FPI temperature sensor based on a mercury-filled silica tube. (SHST: small-hole silica tube, LHST: large-hole silica tube, SMF: single-mode fiber).

The MZI-based temperature sensors could be created by means of splicing a SMF with a thin core fiber or a liquid-filled silica tube [9], [15] and achieved temperature-sensitivities of 51 pm/°C and 6.35 nm/°C [9], [15], respectively. However, these methods usually require complicated fabrication techniques and/or expensive specialty optical fibers.

Temperature sensors based on fiber FPIs were also studied extensively. Various fabrication techniques and structures have been proposed to create fiber FPI temperature sensors, such as by means of laser micro-machining [16], chemical etching [17], applying a miniature end cap [13], [18], [19], applying a multilayer coating [20], and using a micro-mechanical membrane [21]. Nevertheless, the temperature-sensitivities of these devices are relatively low (generally less than 0.40 nm/°C). Recently, a fiber FPI was demonstrated by means of creating an air-bubble in a hollow core fiber (HCF) due to capillary effect of liquid [22]. The device exhibited a high temperature-sensitivity of −6.7 nm/°C, but the fringe contrast was too low for detection, and the fabrication procedure was quite complicated.

In this paper, we propose and demonstrate an ultrasensitive temperature sensor based on a unique fiber Fabry–Pérot interferometer (FPI), which was created by means of splicing a mercury-filled silica tube with a single-mode fiber (SMF). The air cavity of the fiber FPI was formed by the surface of the mercury column and the endface of the SMF. The cavity length of the FPI could be changed by temperature variations due to the thermal expansion of the mercury column. Since the thermal-expansion-coefficient of mercury is up to $1.8 \times 10^{-4}/°C$ at a temperature in the range from 0 °C to 50 °C [23], the proposed sensing architecture demonstrates an ultrahigh temperature-sensitivity of −41.9 nm/°C, which is about one order of magnitude higher than that of the ordinary FPI-based fiber tip sensor reported so far.

2. Device Fabrication and Testing

Fig. 1 illustrates the fabrication process of the proposed mercury-based FPI, which involves six steps. In step 1, as shown in Fig. 1(I), the cleaved end of a smaller hole silica tube (SHST, INNOSEP-TSP040150) with an inner-diameter (ID) of 40 μm and an outer-diameter (OD) of 125 μm, and that of a larger-hole silica tube (LHST, INNOSEP-TSP075150) with an ID of 75 μm and an OD of 125 μm, were placed in the left and the right fiber holder of a commercial available

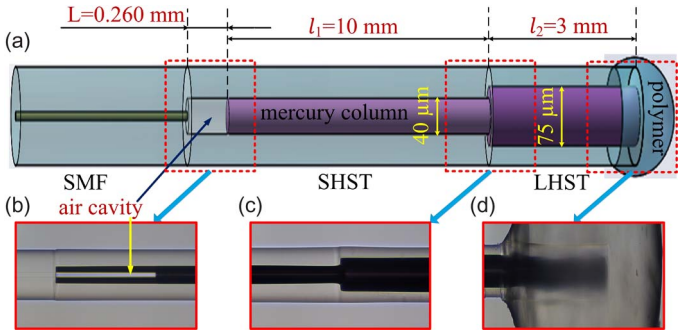

Fig. 2. (a) Schematic diagram of the proposed fiber FPI sensor based on a mercury-filled silica tube. (b) Microscope image of the air cavity of the mercury-based fiber FPI sensor. (c) Microscope image of the spliced joint between the SHST and LHST of the mercury-based fiber FPI sensor. (d) Microscope image of the sealed end from the LHST side of the mercury-based fiber FPI sensor. (Note that the mercury-based fiber FPI sensor has a cavity length of about 260 μm at a temperature of 18 °C.)

fusion splicer (Fujikura FSM-60S), respectively. In step 2, as shown in Fig. 1(I) and (II), the SHST and the LHST were spliced together by means of electrical arc discharge (splicing parameters: fusion power, standard-30 bit; fusion time, 600 ms). In step 3, as shown in Fig. 1(III), the mercury was filled into the silica tube from the LHST side by use of an injector drawing on the SHST side. In step 4, as shown in Fig. 1(IV), the open end of the SHST side of the mercury-filled silica tube was cleaved at the position of 10 mm away from the spliced joint between the SHST and LHST, and then spliced with a standard Corning SMF-28 fiber (splicing parameters: fusion power, standard-20 bit; fusion time, 700 ms). In step 5, as shown in Fig. 1(V), an air cavity was created during the splicing process due to the thermal-induced vaporization of mercury, and thus formed the proposed FPI cavity. Finally, in step 6, as shown in Fig. 1(VI), the open end of the mercury-filled LHST was cleaved to obtain an appropriate length of mercury column, and then the cleaved end was applied with polymer materials (Norland Optical Adhesive 65, http://www.norlandprod.com/adhesives/noa%2065.html) for sealing and protection. It could be seen that the fabricated FPI structure was simple and cost effective.

Furthermore, it should be noted that in step 4 and 5, as shown in Fig. 1(IV) and (V), the heat generated during the electric arc discharge process should be precisely controlled by adjusting the fusion power, the fusion time, and the position of the cleaved end of the SHST. And hence, the thermal-induced vaporization of mercury could be precisely controlled. As a result, we can precisely controlled the air cavity length of the mercury-based FPI and improve the reproducibility of the device.

Fig. 2 illustrates the fabricated mercury-based fiber FPI sensor. The schematic diagram of the mercury-based fiber FPI is shown in Fig. 2(a), it can been seen that the length of SHST, LHST, and FPI air cavity are 10.26, 3.00, and 0.26 mm, respectively, at a temperature of 18 °C. The microscopic images of the air cavity, the spliced joint between the SHST and LHST, and the sealed end from the LHST side of the mercury-based fiber FPI are shown in Fig. 2(b)–(d), respectively. It can be seen from Fig. 2(b) that the surface of mercury column has a curvature due to the existence of surface tension, which is related to the inclination, temperature, air pressure, and roughness of the inner surface of the silica tube.

A broadband light source (BBS) with a wavelength range from 1520 to 1620 nm (i.e., a bandwidth of 100 nm), an optical spectrum analyzer (OSA, YOKOGAWA AQ6370C) with a wavelength resolution of 0.1 nm, and a 3-dB fiber coupler were employed to measure the reflection spectrum of the mercury-based FPI. The typical reflection spectrum of the fabricated mercury-based FPI was measured at the temperature of 23.4 °C, and as shown in Fig. 3, it has a free spectra range (FSR) of 4.9 nm @ 1540 nm and a fringe contrast of 11.75 dB. It should be noted that the 0 dB in Fig. 3 is with respect to the fiber endface reflection of about 4%.

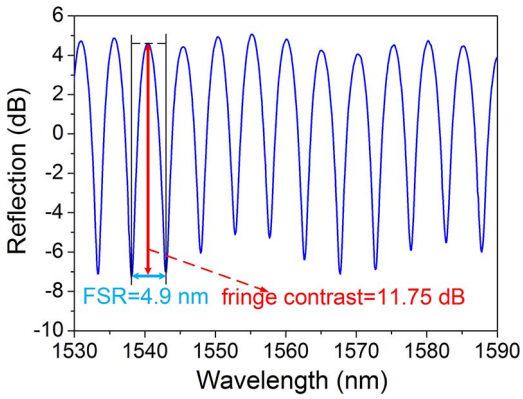

Fig. 3. Reflection spectrum of the mercury-based FPI sensor at a temperature of 23.4 °C.

3. Temperature Response

We investigated the temperature response of the mercury-based FPI sensor via a column oven (LCO 102, temperature stability: ±0.1 °C; see http://www.ecomsro.com/en/s40-product/c9-column-ovens/p60-lco-102-single). The FPI sensor was placed in the oven, and the temperature was raised from 28.4 to 29.4 °C, from 34.1 to 35.0 °C, and from 39.1 to 40.0 °C, respectively. The evolutions of the corresponding reflection spectra of the mercury-based FPI sensor were shown in Fig. 4(a)–(c), respectively. With a temperature rise, the dip wavelengths in the reflection spectra shift towards shorter wavelengths (i.e., so-called "blue" shift). The thermal expansion of the filled mercury reduces the air-cavity length of the FPI, and hence induces the 'blue' shift in dip wavelength. Moreover, as shown in Fig. 4, the fringe contrast also changes with temperature rise, which may result from the temperature-induced variations in the curvature and the reflectivity of the mercury surface. Furthermore, the optical power of light source was attenuated down to 1 mw and the temperature was controlled below 50 °C in the experiments in order to avoid the damage of the temperature sensor due to the excessive volatilization of mercury. We repeated the temperature cycling in a small range of 1 °C for several times and the results could be repeated. No obvious hysteresis could be seen during the temperature cycling. Temperature cycling in a larger range was not carried out due to the limit of the light source bandwidth.

In order to quantitatively investigate the temperature sensitivities of the mercury-based FPI sensor, we depicted the dip wavelengths around 1530, 1535, 1540, and 1545 nm as a function of temperature in different temperature ranges. As shown in Fig. 4(d)–(f), the dip wavelengths exhibit linear "blue" shifts in the small temperature ranges (~1 °C) with temperature rising. In the temperature range from 28.4 to 29.4 °C, the temperature sensitivities of the wavelength dips at 1532.5, 1538.1, 1543.1, and 1548.2 nm are –27.7, –27.8, –28.2, and –28.5 nm/°C, respectively. In the temperature range from 34.1 to 35.0 °C, the temperature sensitivities of the wavelength dips at 1529.2, 1535.0, 1540.8, and 1546.6 nm are –32.1, –32.5, –32.6, and –32.7 nm/°C, respectively. And in the temperature range from 39.1 to 40.0 °C, the temperature-sensitivities of the wavelength dips at 1528.7, 1535.2, 1541.7, and 1548.1 nm are –41.6, –41.6, –41.7, and –41.9 nm/°C, respectively. It can be seen that a linear "blue" shift of the dip wavelengths can be found only in a small temperature range, whereas a nonlinear "blue" shift will be found in a larger temperature range. Moreover, a higher temperature-sensitivity will be achieved when the mercury-based FPI sensor is operated at higher temperatures.

The reflected optical intensity of the proposed mercury-based FPI temperature sensor can be expressed as

$$I = I_1 + I_2 + 2\sqrt{I_1 I_2}\cos\varphi \tag{1}$$

$$\varphi = \frac{4\pi nL}{\lambda} \tag{2}$$

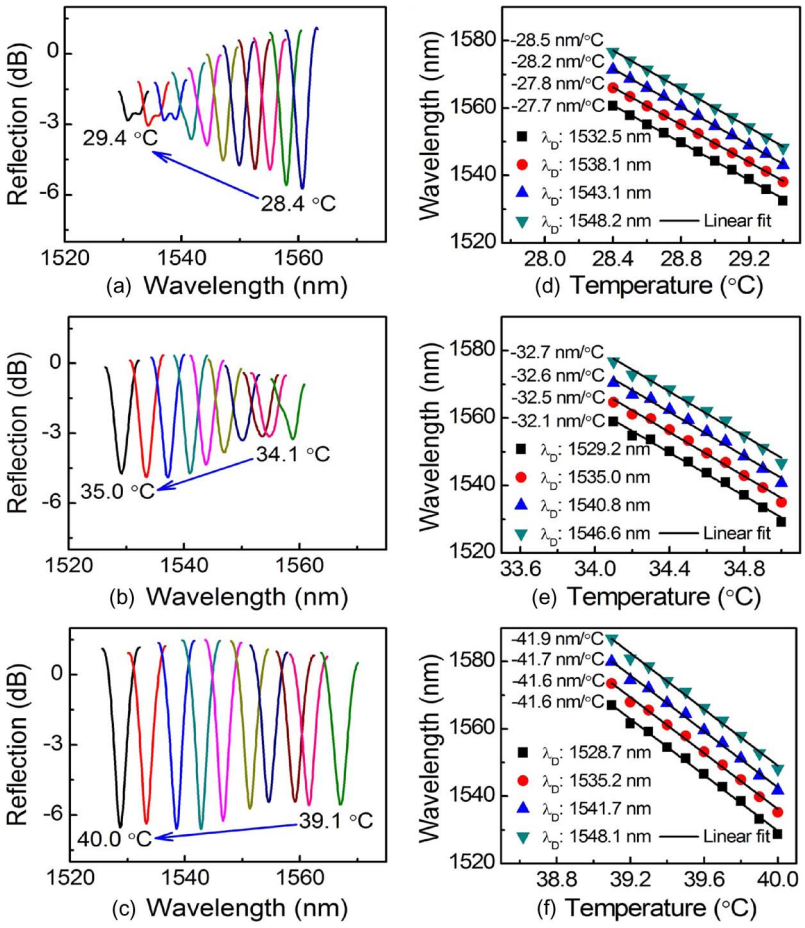

Fig. 4. Reflection spectra evolution of the mercury-based FPI sensor with the temperature rise in different temperature ranges of (a) from 28.4 to 29.4 °C, (b) from 34.1 to 35.0 °C, and (c) from 39.1 to 40.0 °C, respectively, at an interval of 0.1 °C, and the corresponding wavelength shifts of the dip wavelengths (λ_D) around 1530, 1535, 1540, and 1545 nm as a function of temperature in different temperature ranges of (d) from 28.4 to 29.4 °C, (e) from 34.1 to 35.0 °C, and (f) from 39.1 to 40.0 °C, respectively.

where I_1 and I_2 are the intensities of two beams reflected by the SMF endface and the surface of mercury column, respectively. φ is the phase difference between the two beams induced by the air cavity, L is the air cavity length, n is the refractive index of the air, and λ is the inspected wavelength in vacuum. The phase difference satisfies the resonance condition

$$\varphi = (2k+1)\pi \quad (k \text{ is an integer}). \tag{3}$$

By choosing two dip wavelengths that satisfy the resonance condition in an interference fringe, λ_1 $(k = m + x)$ and λ_2 $(k = m)$, the air-cavity length L can be calculated from the measured interference fringes as

$$\frac{4\pi nL}{\lambda_1} - \frac{4\pi nL}{\lambda_2} = [2(k+x)+1]\pi - (2k+1)\pi = 2x\pi \tag{4}$$

and the air-cavity length L can be expressed as

$$L = \frac{\lambda_1 \lambda_2 x}{2n(\lambda_2 - \lambda_1)}. \tag{5}$$

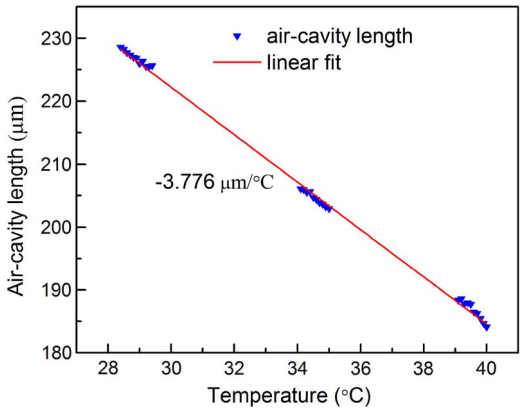

Fig. 5. Air-cavity length evolution of the mercury-based FPI sensor as a function of the temperature rise.

We calculated the air cavity length by use of (5) and the previous experimental results in temperature ranges of 28.4–29.4 °C, 34.1–35.0 °C, and 39.1–40.0 °C. According to the linear fits of the experimental results, as shown in Fig. 4, it can be seen that the air-cavity length L responds linearly to the temperature change with a sensitivity of -3.776 μm/°C, i.e., the air-cavity length L is decreased by 3.776 μm with a temperature increase of 1 °C.

4. Discussions

4.1 Theoretical Analysis of the Temperature Sensitivity

The air-cavity length L discussed above was calculated from the experimentally-measured interference fringes. Moreover, the air-cavity length can also be theoretically calculated from the viewpoint of the expansion of mercury, since the change in the air-cavity length mainly originates from the expansion of mercury column. As shown in Fig. 2(a), the volume of the mercury column can be given by

$$V = l_1 \pi r_1^2 + l_2 \pi r_2^2 \tag{6}$$

where l_1, l_2, and r_1, r_2 are the length and radius of the SHST and LHST, respectively, and the temperature-induced expansion of mercury column should be

$$\Delta V = V \gamma \Delta T \tag{7}$$

where ΔV is the volume expansion value of the mercury column, ΔT is the temperature change, and γ is the thermal expansion coefficient of mercury. Hence, the change in air-cavity length can be derived from (7) and is expressed as

$$\Delta L_e = -\frac{\Delta V}{s} = -\frac{\Delta V}{\pi r_1^2} \tag{8}$$

where Le is the air-cavity length induced by the expansion of mercury, and s is cross-section area of the mercury column in the SHST. We substitute (6) and (7) into (8), and then, the differentiation is done. Therefore, the temperature-induced change of the air-cavity length Le should be

$$\frac{dL_e}{dT} = -\frac{(l_1 \pi r_1^2 + l_2 \pi r_2^2)\gamma}{\pi r_1^2} = -\gamma \left(l_1 + l_2 \left(\frac{r_2}{r_1} \right)^2 \right). \tag{9}$$

As shown in Fig. 2(a), l_1, l_2, r_1, and r_2 are 10 mm, 3 mm, 20 μm, and 37.5 μm, respectively. γ is the thermal expansion coefficient of mercury, and it is almost a constant (i.e., $1.8 \times 10^{-4}/^{\circ}$C) in the temperature range of 0–50 °C. By substituting these values into (9), we can calculate the temperature-induced change of air-cavity length as $dL_e/dT = -3.700$ μm/°C, and this theoretically-predicted value (i.e., $dL_e/dT = -3.700$ μm/°C) agrees well with the experimental result (i.e., $dL/dT = -3.776$ μm/°C, as shown in Fig. 5). It should be noted that the influence of pressure change in the air cavity was ignored in the previous discussions.

Moreover, it could be seen from (9) that compared with the FPIs based on a single LHST or a single SHST, the employment of the combination of a LHST and a SHST in this paper can drastically increase the temperature sensitivity of the mercury-based FPI sensor with a given sensing length.

4.2 Analysis of the Fringe Contrast

The fringe contrast could be analyzed via (1). I1 and I2 are the intensities of two beams reflected by the SMF endface and the surface of mercury column, respectively. Due to the much higher reflectivity of the mercury surface (up to 79.5% in a wavelength range of 1500~1600 nm) than that of the SMF endface (i.e., ~ 4%), the enhanced reflection of the mercury surface can partially overcome the air cavity loss and match well with the reflection of SMF endface, thus giving rise to an excellent fringe contrast (i.e., 11.75 dB) in the reflection spectrum. Moreover, the reflectivity of the mercury surface is much higher than that of the other liquids, such as water, alcohol, and kerosene. And hence, a much larger optical power could be detected in the proposed mercury-based FPI than that of a previously-reported water-based FPI [24].

Furthermore, in the case of a small temperature change of 1 °C, the central section of the mercury surface moves forward at a significant distance of 3.70 μm and leads to the changes in the curvature and the reflectivity of the mercury surface. The reflection on the mercury surface is then collected by an ordinary SMF at a distance of 260 μm away (i.e., the air cavity length), and hence the air cavity loss of the FPI should be sensitive to any tiny variations in the curvature and the reflectivity of the mercury surface. As a result, as shown in Fig. 4(a), the fringe contrast varied drastically during a small temperature change of only 1 °C.

4.3 Important Issues of the Mercury-Based FPI Sensors for Applications

Sensitivity and Resolution

As discussed above, the proposed mercury-based FPI sensor has a maximum temperature sensitivity of –41.9 nm/°C, which is nearly one order of magnitude higher than those of the previous reported FPI-based temperature sensors using wavelength demodulation [13], [14], [16]–[22]. It can further be calculated from (2) and Fig. 5 that the temperature sensitivity is 30.6 rad/°C, which is also much higher than those of the FPI-based temperature sensors using phase demodulation [25]. In this paper, we used an OSA to demodulate the wavelength-shift of the FPI sensor. The wavelength resolution was 0.1 nm. As a result, the temperature resolution of the proposed mercury-based FPI sensor should be 0.0067 °C. Nevertheless, the wavelength resolution could further be improved by use of a high-resolution wavelength/phase demodulator together with a dip-seeking algorithm.

Ambiguity, Linearity, and Operation Range

As shown in Figs. 3 and 4, due to the periodic nature of the spectra, the fringe ambiguity will occur even in a small temperature range of 0.2 °C. Moreover, it can be seen from (5) and Fig. 4 that the temperature response of the FPI sensor using wavelength modulation is intrinsically nonlinear in a large temperature range, i.e., the temperature sensitivity is larger at a higher temperature. The ambiguity and the nonlinearity could easily be overcome by using phase demodulation together with a fringe counter and an initial temperature reference, and hence, the temperature range for operation could be enlarged.

The Use of Mercury

The structure of the mercury-based FPI temperature sensor proposed in this paper is very similar to a traditional mercury-based thermometer. By using the optical method, nanometer-level deformations could be observed, and hence a high temperature-sensitivity could be achieved. Due to the large thermal expansion coefficient and the high reflectivity of the surface, the mercury plays an important part in the FPI temperature sensor. However, the mercury is toxic. We can reduce the amount of mercury and seal it in the silica tube with polymer materials to minimize its harm to the environment and the human body.

5. Conclusion

We demonstrate a fiber Fabry–Pérot interferometer for temperature sensing with ultrahigh sensitivity. By splicing a mercury-filled silica tube with a single mode fiber, an air cavity is formed and acts as a FPI cavity. Such a FPI cavity can be compressed by the thermal expansion of the mercury column, and exhibits an ultrahigh temperature-sensitivity of ~41.9 nm/°C at the temperature around 40 °C and a temperature sensing range of 0–50 °C. The proposed mercury-based FPI temperature sensor is expected to have potential applications in highly-sensitive temperature sensing, for example, monitoring the environmental temperature in the biological processes.

References

[1] C. Chen *et al.,* "Monitoring thermal effect in femtosecond laser interaction with glass by fiber Bragg grating," *J. Lightw. Technol.*, vol. 29, no. 14, pp. 2126–2130, Jul. 2011.

[2] J. He *et al.,* "Highly birefringent phase-shifted fiber Bragg gratings inscribed with femtosecond laser," *Opt. Lett.*, vol. 40, no. 9, pp. 2008–2011, May 2015.

[3] C. R. Liao, Y. H. Li, D. N. Wang, T. Sun, and K. T. V. Grattan, "Morphology and thermal stability of fiber Bragg gratings for sensor applications written in H_2-free and H_2-loaded fibers by femtosecond laser," *IEEE Sensors J.*, vol. 10, no. 11, pp. 1675–1681, Nov. 2010.

[4] Y. P. Wang, "Review of long period fiber gratings written by CO_2 laser," *J. Appl. Phys.*, vol. 108, no. 8, Nov. 2010, Art. ID. 081101.

[5] Y. J. Rao, Y. P. Wang, Z. L. Ran, and T. Zhu, "Novel fiber-optic sensors based on long-period fiber gratings written by high-frequency CO_2 laser pulses," *J. Lightw. Technol.*, vol. 21, no. 5, pp. 1320–1327, May 2003.

[6] G. L. Yin *et al.,* "Long period fiber gratings inscribed by periodically tapering a fiber," *IEEE Photon. Technol. Lett.*, vol. 26, no. 7, pp. 698–701, Apr. 2014.

[7] Y. Liu *et al.,* "Compact tunable multibandpass filters based on liquid-filled photonic crystal fibers," *Opt. Lett.*, vol. 39, no. 7, pp. 2148–2151, Apr. 2014.

[8] Y. Wang, M. Yang, D. N. Wang, and C. R. Liao, "Selectively infiltrated photonic crystal fiber with ultrahigh temperature sensitivity," *IEEE Photon. Technol. Lett.*, vol. 23, no. 20, pp. 1520–1522, Oct. 2011.

[9] J. Zhou *et al.,* "Simultaneous measurement of strain and temperature by employing fiber Mach-Zehnder interferometer," *Opt. Exp.*, vol. 22, no. 2, pp. 1680–1686, Jan. 2014.

[10] D. Chen and X. Jiang, "All-fiber temperature sensor based on few mode fiber and single-mode fiber," *Microw. Opt. Technol. Lett.*, vol. 55, no. 7, pp. 1700–1703, Jul. 2013.

[11] J. He *et al.,* "High-sensitivity temperature sensor based on a coated single-mode fiber loop," *J. Lightw. Technol.*, vol. 33, no. 19, pp. 4019–4026, Oct. 2015.

[12] C. R. Liao, H. F. Chen, and D. N. Wang, "Ultra compact optical fiber sensor for refractive index and high temperature measurement," *J. Lightw. Technol.*, vol. 32, no. 14, pp. 2531–2535, 2014.

[13] X. Y. Zhang *et al.,* "Miniature end-capped fiber sensor for refractive index and temperature measurement," *IEEE Photon. Technol. Lett.*, vol. 26, no. 1, pp. 7–10, Jan. 2014.

[14] Y. Zhao, D. Wang, and R. Lv, "A novel optical fiber temperature sensor based on Fabry-Perot cavity," *Microw. Opt. Technol. Lett.*, vol. 55, no. 10, pp. 2487–2490, Oct. 2013.

[15] A. Zhou, Y. Zhang, Q. Xu, J. Yang, and L. Yuan, "Semi-open cavity in-fiber Mach-Zehnder interferometer for temperature measurement with ultra-high sensitivity," *Appl. Opt.*, vol. 53, no. 12, pp. 2696–2701, Apr. 2014.

[16] T. Wei, Y. K. Han, H. Tsai, and H. Xiao, "Miniaturized fiber inline Fabry-Perot interferometer fabricated with a femtosecond laser," *Opt. Lett.*, vol. 33, no. 6, pp. 536–538, Mar. 2008.

[17] X. Chen, F. Shen, Z. Wang, Z. Huang, and A. Wang, "Micro-air-gap based intrinsic Fabry-Perot interferometric fiber-optic sensor," *Appl. Opt.*, vol. 45, no. 30, pp. 7760–7766, Oct. 2006.

[18] B. Sun *et al.,* "Simultaneous measurement of pressure and temperature by employing Fabry-Perot interferometer based on pendant polymer droplet," *Opt. Exp.*, vol. 23, no. 3, pp. 1906–1911, Feb. 2015.

[19] J. Wang, S. L. Wu, and W. Y. Ren, "Simultaneous measurement of refractive index and temperature using an epoxy resin-based interferometer," *Appl. Opt.*, vol. 53, no. 33, pp. 7825–7830, Nov. 2014.

[20] D. W. Lee, Z. P. Tian, J. X. Dai, W. B. Hu, and M. H. Yang, "Sapphire fiber high-temperature tip sensor with multilayer coating," *IEEE Photon. Technol. Lett.*, vol. 27, no. 7, pp. 741–743, Apr. 2015.

[21] Y. Liu, W. Tian, and J. Hua, "Fiber temperature sensor based on micro-mechanical membranes and optical interference structure," in *Proc. 3rd Int. POEM*, vol. 276, no. 1, 2011, Art. ID. 012151.
[22] C. L. Lee *et al.,* "Fiber Fabry-Perot interferometers based on air-bubbles/liquid in hollow core fibers," *IEEE Photon. Technol. Lett.*, vol. 26, no. 8, pp. 749–752, Apr. 2014.
[23] M. Kumari and N. Dass, "Volume and thermal expansion of mercury in the temperature range 0–150 °C & pressure range 0–8 K bar," *J. Non-Crystalline Solids*, vol. 117/118, pp. 563–566, Feb. 1990.
[24] Y. Wang, D. N. Wang, C. Wang, and T. Hu, "Compressible fiber optic micro-Fabry-Perot cavity with ultra-high pressure sensitivity," *Opt. Exp.*, vol. 21, no. 12, pp. 14084–14089, Jun. 2013.
[25] W. H. Tsai and C. J. Lin, "A novel structure for the intrinsic Fabry-Perot fiber-optic temperature sensor," *J. Lightw. Technol.*, vol. 19, no. 5, pp. 682–686, May 2001.